A Mathematical Model of Wire Feeding Mechanisms in GMAW

Investigations into both aluminum and steel welding wire focus on elements that contribute to poor feedability

BY T. M. PADILLA, T. P. QUINN, D. R. MUNOZ, AND R. A. L. RORRER

ABSTRACT. A Hertzian-based contact model of the friction between the welding wire and the wire liner has been developed to predict the wire pulling force for gas metal arc welding (GMAW). The model predicts a 2.5:1 exponential increase in wire pulling force as the bend angle between the welding wire and the wire liner is varied from 0 to 180 deg. A one-dimensional force transducer recorded the wire pulling force, while a linear actuator pulled the welding wire through various wire liners at constant wire feed speeds ranging from 10 to 18 m/min (400 to 700 in./min). Results indicate model agreement to within ± 0.60 N (0.14 lbf) RMS when using aluminum welding wires ranging from 0.8 to 1.6 mm (0.030 to 0.0625 in.) in diameter. Extension of the model to applications feeding steel welding wires exhibits agreement to within ± 0.80 N (0.18 lbf) RMS when using 1.1-mm-diameter (0.045-in.) welding wires and a spiral-wound steel wire liner. Statistical analyses show an independence of wire pulling force from wire feed speed over the interval of speeds ranging from 10 to 18 m/min (400 to 700 in./min).

Introduction

A key factor in the performance of gas metal arc welding (GMAW) is the feedability of the welding wire through the wire liner. For aluminum electrodes, fluctuations in the wire feed speed (WFS) of even 1% can lead to irregular arc lengths, oscillatory voltage and current levels, and degradation of the overall weld quality (Ref. 1). In part, variations in the target WFS are caused by adverse conditions during welding (Refs. 2–4). These include damaging effects such as "stick-slip" motion of the welding wire, premature wear of the contact tube and, in general, uncontrolled movement of the hose package during welding. A considerable amount of effort (Refs. 5–9) has been spent to develop microprocessor-based wire delivery systems and specialized components that are capable of reducing velocity variations to within 0.5 to 1.0% of the target value. Here, these specialized components and processes allow for controlled feeding at distances of up to 60 m (200 ft) between the wire spool and the workpiece. However, the use of such systems is an expensive and nontrivial option when compared to conventional means of wire delivery (Ref. 10), thereby leaving room for more practical and cost-effective solutions.

At present, a limited amount of published research has been conducted to understand and separate the various elements that contribute to poor wire feeding performance. One important factor that controls wire feedability is friction between the welding wire and the wire liner. Large or irregular wire feeding forces have been shown (Refs. 3 and 4) to cause pronounced fluctuations in the WFS and wire buckling. These problems are more readily manifested when feeding aluminum and other difficult-to-feed alloys (Ref. 11). Studies have been conducted (Refs. 6 and 12) to measure the wire feeding force during welding, but a limited amount of detail has been given to model the source of friction. This paper presents a Hertzian-based contact model of the welding wire-to-wire liner friction as the welding wire is pulled through various wire liners at constant velocity.

KEY WORDS

Aluminum Wire Feeding
Friction Model
GMAW Wire Feeding
Hertzian Contact Mechanics
Steel Wire Feeding
Wire Feeding Force
Wire Friction

Model

Movement of the welding wire through the wire liner is similar to "belt-on-drum" applications — Fig. 1. Historically, this situation has been treated using Euler's equation (Ref. 13) for rope friction given by

$$T_2 = T_1 e^{\mu\theta} \qquad (1)$$

where T_1 refers to the slack-side tension, T_2 the tight-side tension, μ the wire-to-liner coefficient of friction, and θ the wire-to-liner contact angle.

Predictions of the wire-to-liner friction force using Euler's equation rely on the use of known values for the coefficient of friction. Even when the formulations of the welding wire and wire liner materials are known (most are proprietary), little data exists for the coefficient of friction in the context of a wire sliding on a stationary surface. Predictions can be made using the coefficient of friction from similar materials, but these predictions do not adequately fit the experimental results and either overestimate or underestimate the true functional form of the data (Ref. 14).

An alternative model utilizing aspects of Hertzian contact mechanics and friction theory has been developed to better predict the wire-to-liner friction using only basic information about the welding wire and the wire liner. The alternative model is based upon experimentally determining the shear strength at the welding wire and wire liner interface. As a result, there is no need to rely on tabulated data for the co-

T. M. PADILLA and D. R. MUNOZ are with Colorado School of Mines, Division of Engineering, Golden, Colo. T. P. QUINN is with National Institute of Standards and Technology, Materials Reliability Division, Boulder, Colo. R. A. L. RORRER is with University of Colorado at Denver, College of Engineering, Denver, Colo.

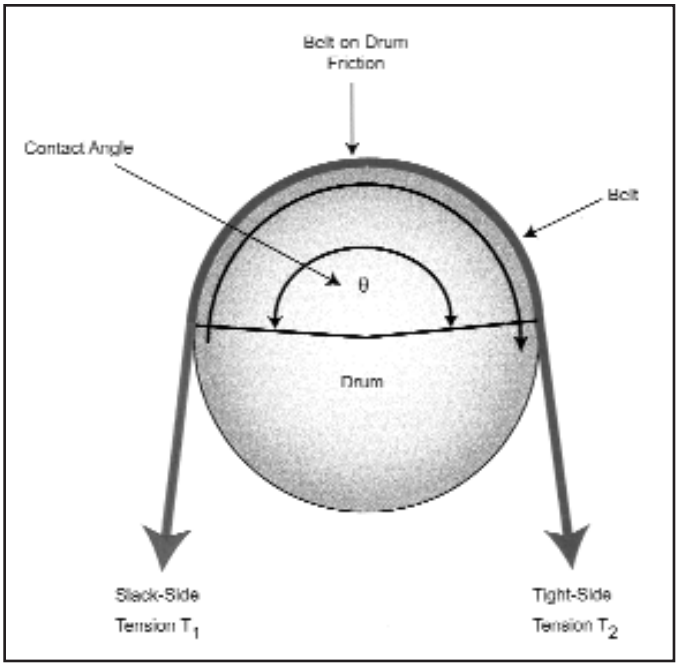

Fig. 1 — Schematic of Euler's rope friction equation for "belt-on-drum" applications.

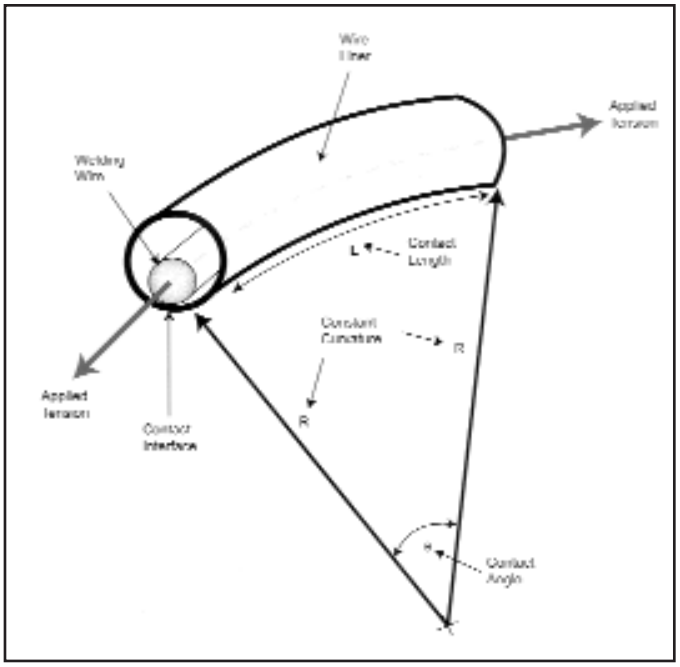

Fig. 2 — The welding wire and wire liner modeled as a pair of axially aligned cylinders under constant curvature and with a specified contact angle.

efficient of friction since an actual interface parameter can be computed for any welding wire and wire liner pair. The following details this development.

According to Hertzian contact theory, when two rough surfaces come in contact with each other, the surfaces distort locally and make contact at discrete points (Ref. 15). In the case of the welding wire and the wire liner, the combination can be modeled as a pair of axially aligned cylinders that make contact under constant curvature *R*, and with a specified "wrap" or contact angle θ — Fig. 2.

If a differential element of the welding wire is pulled with applied tensions T_1 and T_2 (Fig. 3) at steady-state conditions (with assumed constant velocities and negligible accelerations) over constant curvature *R* and through a fixed contact angle θ, the distributed load *w* acting per unit length over the segment of welding wire can be formulated from a static force balance. Considering the arbitrary orientation of a differential segment of the welding wire (Fig. 3), the equations of equilibrium can be written as

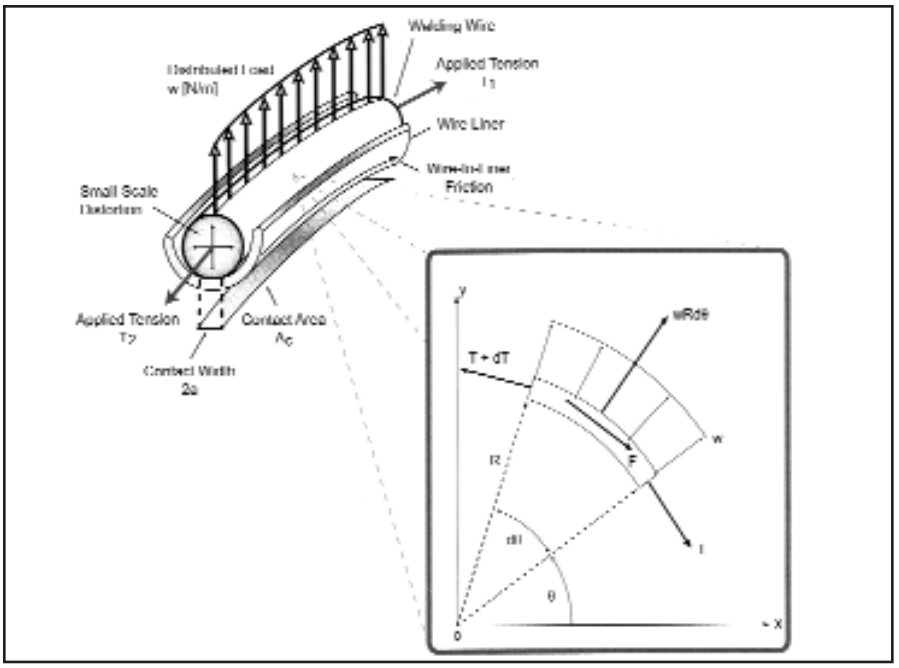

Fig. 3 — A segment of the welding wire and the wire liner showing the contact area caused by the applied tensions T_1 and T_2.

$$\sum F_x = 0;$$
$$T\sin\left(\theta\right) + wRd\theta\cos\left(\theta + \frac{d\theta}{2}\right) + F\sin\left(\theta + \frac{d\theta}{2}\right) - \left(T + dT\right)\sin\left(\theta + d\theta\right) = 0 \quad (2)$$

$$\sum F_y = 0;$$
$$-T\cos\left(\theta\right) + wRd\theta\sin\left(\theta + \frac{d\theta}{2}\right) - F\cos\left(\theta + \frac{d\theta}{2}\right) + \left(T + dT\right)\cos\left(\theta + d\theta\right) = 0 \quad (3)$$

$$\sum M_o = 0;$$
$$FR + TR - \left(T + dT\right)R = 0\,. \quad (4)$$

Here, the angle θ refers to the initial start position of curvature as measured from the abscissa, *d*θ refers to subtended angle of the differential element, *T* the applied welding wire tension, *dT* the additional

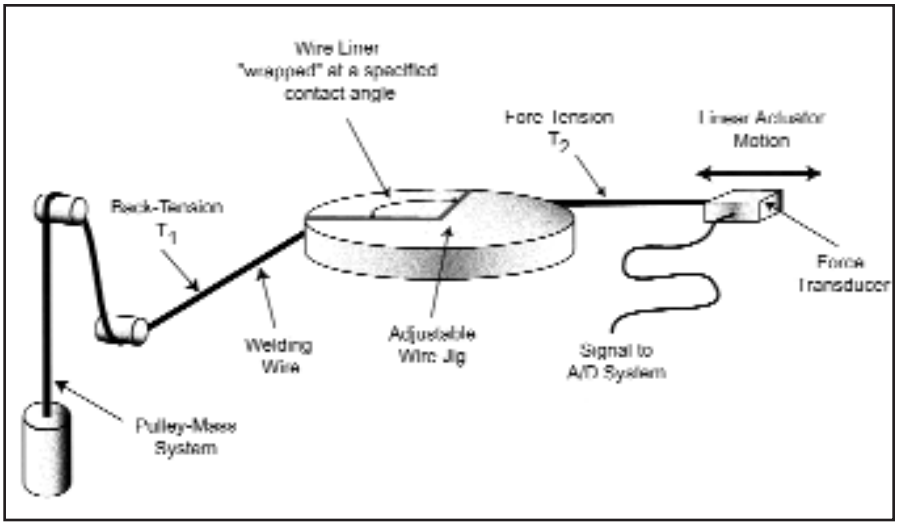

Fig. 4 — Experimental apparatus used to measure the pulling force as the welding wire slides through the wire liner.

tension due to the tangential resistive force *F*, *R* the constant bend radius of curvature, and *w* the distributed loading acting over the differential element of the welding wire.

By small angle theory (Ref. 16), as the value of $d\theta$ approaches zero, the sine and cosine terms containing the $d\theta$ argument behave as

$$\lim_{d\theta\to 0} \sin(d\theta) = d\theta$$
$$\lim_{d\theta\to 0} \cos(d\theta) = 1. \quad (5)$$

Using Equation 5 with Equations 2–4 and simplifying to include only first order terms results in equilibrium equations of the form

$$wRd\theta\cos(\theta) + F\left[\sin(\theta) + \cos(\theta)\left(\frac{d\theta}{2}\right)\right] - Td\theta\cos(\theta) - dT\sin(\theta) = 0 \quad (6)$$

$$wRd\theta\sin(\theta) - F\left[\cos(\theta) - \sin(\theta)\left(\frac{d\theta}{2}\right)\right] - Td\theta\sin(\theta) + dT\cos(\theta) = 0 \quad (7)$$

$$F - dT = 0. \quad (8)$$

Adding Equation 6 to Equation 7 and substituting Equation 8 upon simplification to retain first order terms yields

$$wR\sin(\theta) + wR\cos(\theta) - T\cos(\theta) - T\sin(\theta) = 0. \quad (9)$$

Gathering like terms to solve for the distributed loading *w* acting over the differential element provides

$$w = \frac{T}{R}, \quad (10)$$

where the tension *T* is a function of the

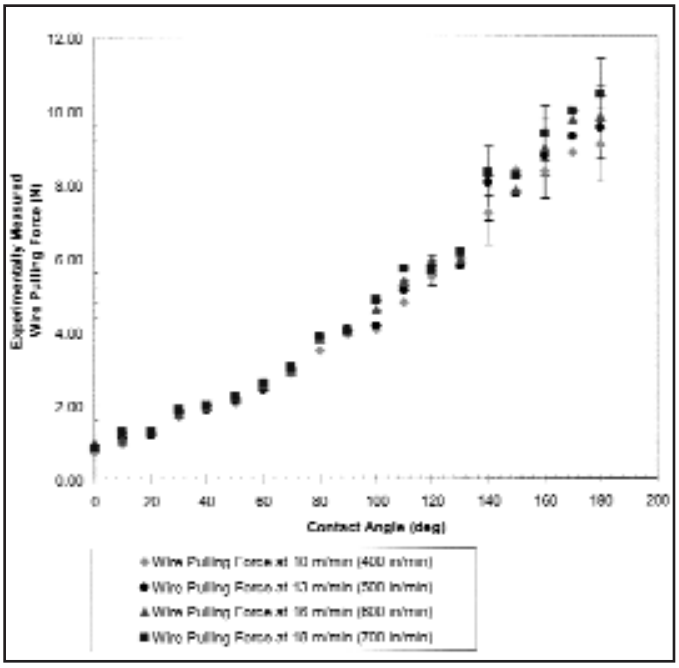

Fig. 5 — Wire pulling force for WFS = 10 to 18 m/min (400 to 700 in./min) with a 0.8-mm (0.030-in.) ER5356 solid-core aluminum welding wire dry-sliding on a 1.3-mm (0.052-in.) internal diameter Teflon wire liner. The data shown have been normalized for a 5-N (1.1-lbf) uniform backtension to show a nonzero force value at zero contact angle representing static friction.

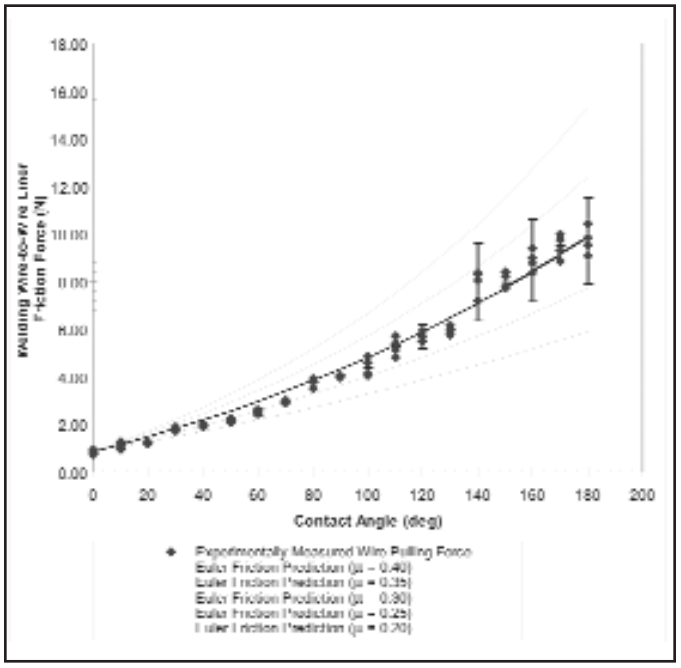

Fig. 6 — Wire pulling force using the Euler rope friction equation for WFS = 10 to 18 m/min (400 to 700 in./min) with a 0.8-mm (0.030-in.) ER5356 solid-core aluminum welding wire dry-sliding on a 1.3-mm (0.052-in.) internal diameter Teflon wire liner. The predicted force values are for representative wire/liner systems having a range of coefficient of friction values from μ = 0.2 to 0.4.

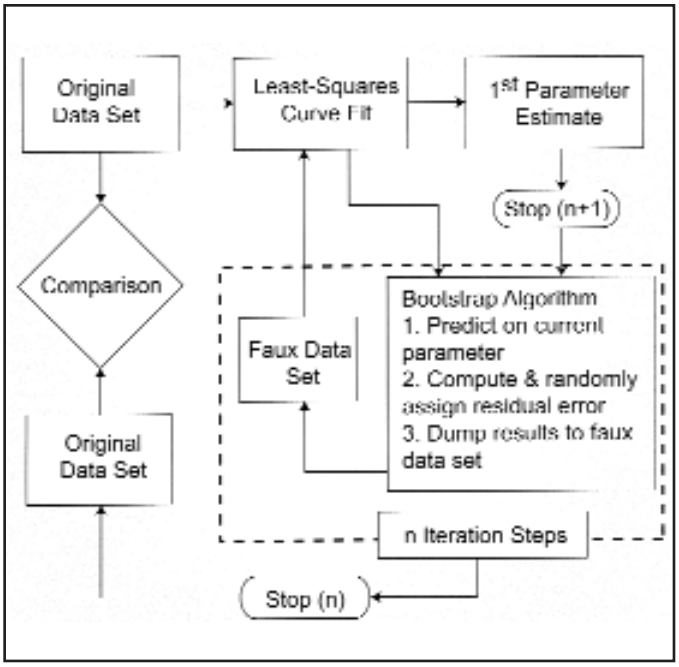

Fig. 7 — Process flowchart showing the steps of the Bootstrap algorithm used to determine the interfacial shear strength between the welding wire and the wire liner.

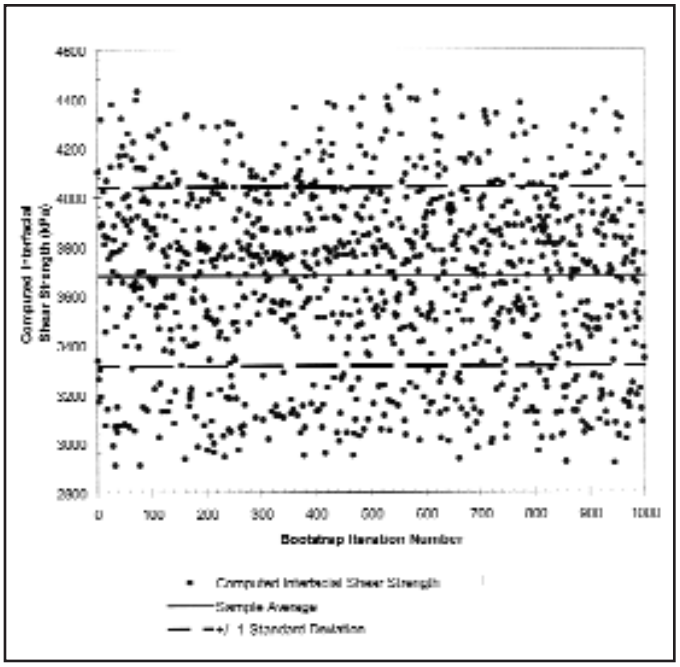

Fig. 8 — Sample scatter plot of an arbitrary data set using 1000 iterations of the Bootstrap algorithm to generate a sample average and standard deviation in the interfacial shear strength.

contact angle θ and the bend radius R is assumed constant over the entire contact angle range. According to Hertzian contact theory, the applied loading and subsequent surface deformation of bodies in contact create an area of contact A_c that can be expressed in terms of the semi-infinite half-width a and the wire-to-liner contact length L (Ref. 17) as

$$A_c = 2\,aL. \tag{11}$$

In this expression, L is taken as the segment length of the differential element through the subtended angle $d\theta$. Assuming the radius of curvature R for the differential element is constant, the segment length L can be written as

$$L = Rd\theta. \tag{12}$$

For axially aligned, conformal cylinders, the Hertzian-based semi-infinite half-width a of Equation 11 is defined (Ref. 17) as

$$a = \sqrt{\frac{4wR'}{\pi E^*}}, \tag{13}$$

where R' and E^* refer, respectively, to the reduced radius of curvature and the effective surface modulus of the mating bodies. In this expression, w is the applied uniform distributed loading acting along the body-to-body contact length of the differential element calculated earlier in Equation 10.

The quantities R' (adjusted with a negative sign to account for conformal bodies) and E^* of Equation 13 can be formulated in terms of the material properties designated by Poisson's ratio ν, Young's modulus E, and the nominal welding wire and wire liner radii of curvature r. Using the indices "w" and "l" to designate nominal properties associated with the welding wire and the wire liner, respectively, E^* and R' (Ref. 17) can be expressed as

$$E^* = \left(\frac{1-\upsilon_w^2}{E_w} + \frac{1-\upsilon_l^2}{E_l}\right)^{-1} \tag{14}$$

$$R' = \left(\frac{1}{r_w} + \frac{1}{-r_l}\right)^{-1}. \tag{15}$$

By Amontons' Law (Ref. 17) for friction, the measure of resistance to motion (i.e., μ the coefficient of friction) is normally defined to be independent of the apparent contact area and in terms of the normal force N and tangential resistive force F, such that

$$\mu = \frac{F}{N}. \tag{16}$$

However, since real surfaces are known to contain irregularities in their surface topology, the theoretical coefficient of friction can be shown (Refs. 15, 17–19) to be dependent on the "real" contact area caused by surface distortion and asperity-to-asperity contact. Accordingly, Equation 16 can be re-expressed as a function of the real contact area A_c to give

$$\mu = \mu(A_c). \tag{17}$$

For the welding wire to wire liner contact, the normal load N of Equation 16 is a quantity that depends only on the applied tension and is independent of the body-to-body contact area. This leaves the tangential resistive force F as the term responsible for the area dependency in the coefficient of friction observed in Equation 17. Elementary friction theory further suggests the total resistance to motion for rough surfaces can be summed over all asperity-to-asperity contacts (essentially the mating contact area A_c, if statistical variations are ignored) provided the interfacial shear strength between the mating materials remains constant (Refs. 15, 17–19). Hence, the tangential resistive force F acting between the welding wire and the wire liner can be written in terms of the real contact area A_c, and the wire-to-liner interfacial shear strength τ as

$$F = A_c\,\tau. \tag{18}$$

By the simplified equations of equilibrium given in Equations 6–8, the tangential resistive force F is equivalent to the change

Table 1 — Summary of the Values and Conditions Used in Case Studies

Item	Case Study No. 1	Case Study No. 2	Case Study No. 3
Test Summary	Manufacturer Matched Aluminum-on-Teflon	Manufacturer Matched Aluminum-on-Nylon	Manufacturer Matched Steel-on-Steel
	Welding Wire		
Alloy	Solid-Core Aluminum ER5356	Solid-Core Aluminum ER5356	Solid-Core Copper-Clad Steel ER70S6
Nominal Diameter	0.8 mm (0.030 in.)	1.6 mm (0.0625 in.)	1.1 mm (0.045 in.)
	Wire Liner		
Composition	Polymer Based, Teflon Impregnated	Polymer Based, Nylon Impregnated	Mild Steel, Spirally Wound
Nominal Internal Diameter	1.3 mm (0.052 in.)	2.5 mm (0.100 in.)	1.7 mm (0.065 in.)
Wire Liner I.D. to Welding Wire O.D. Ratio	1.7:1	1.6:1	1.4:1
Wire Feed Speed	10 to 18 m/min (400 to 700 in./min) @ 2.5 m/min (100 in./min) increments	Single Constant-Valued: 14 m/min (550 in./min)	10 to 18 m/min (400 to 700 in./min) @ 2.5 m/min (100 in./min) increments
Contact Angle	0 to 180 deg in 10-deg increments	0 to 180 deg in 10-deg increments	0 to 180 deg in 10-deg increments
Applied Backtension	5 N (1.1 lbf)	5 N (1.1 lbf)	10 N (2.2 lbf)
Wire-to-Liner Sliding Condition	Dry, as manufactured	Dry, as manufactured	Dry, as manufactured

on tension dT acting over the differential segment of the welding wire. Equating these quantities results in,

$$dT = F$$
$$\therefore dT = A_c \tau . \quad (19)$$

Substituting the expression for the contact area A_c and the following terms L, a, R', E^*, and w as developed earlier, results in

$$dT = 4\tau \sqrt{\frac{TRR'}{\pi E^*}} d\theta . \quad (20)$$

Dividing Equation 21 by the quantity $d\theta$ produces a first order nonlinear homogenous ordinary differential equation of

$$\frac{dT}{d\theta} - 4\tau \sqrt{\frac{TRR'}{\pi E^*}} = 0. \quad (21)$$

Solving Equation 21 by separation of variables and integrating over the differential element, as shown in Fig. 3, results in the following relationship between the applied backtension T_1, the applied fore tension T_2, and the interfacial shear strength τ.

$$T_2 = \left[T_1^{1/2} + 2\tau\left(\theta_1 - \theta_2\right)\sqrt{\frac{RR'}{\pi E^*}} \right]^2 \quad (22)$$

Here, the quantities T_1, R, θ_1, θ_2, R', and E^* can either be obtained directly or computed from the initial wire-to-liner setup, thereby leaving τ as an unknown parameter that can be determined empirically. The end result is an alternative model to the Euler rope friction equation that is independent of the nominal coefficient of friction and that is capable of predicting the wire pulling force given only basic information about the welding wire and wire liner system.

Experiments

Full-scale tests were conducted to determine the validity of the contact model developed in this research. The welding wire and the wire liner were wrapped around a variable-angle jig (Fig. 4) to simulate a combination of bends typically found in the wire-feeding hose package. One end of the welding wire was attached to a pulley and mass system to create a uniform backtension on the welding wire, thereby simulating the drag normally associated with the wire spool. The uniform backtension also helps ensure complete contact of the welding wire with the wire liner.

Travel speed of the welding wire through the wire liner is controlled using a computer-driven linear actuator that is capable of providing a stroke of 3 m (10 ft) at velocities ranging from 0.01 to 30.5 m/min (0.5 to 1200 in./min) to within ± 0.5% absolute. Once a particular combination of the welding wire, wire liner, wire feed speed, and bend curvature was selected, the linear actuator was initiated and triggered a data-acquisition system to record the wire pulling force. The force transducer used in this application is capable of measuring up to 110 N (25 lbf) with an uncertainty of ± 0.05% full-scale as computed from a static calibration. Following a force measurement, the wire jig was reset to a new contact angle and the experiment was repeated.

In this study, three individual cases were considered to determine the accuracy of the contact model in predicting the wire pulling force when using various combinations of readily available welding wires and wire liners. In each case study, the welding wire was initially unspooled with a wire cast[1] radius of approximately 50 mm (2 in.) and subsequently straightened to a cast radius of approximately 1.2 m (48 in.). Helix[1] in the welding wire was measured to be less than 13 mm (0.5 in.) and was considered to be negligible. The surface of the welding wire and the wire liner was dry, unlubricated, and used in the as-manufactured condition. Replication measurements (shown as data error bars in attached figures) were taken for statistical analysis at wire-to-liner contact angles equal to 0, 60, 120, 140, 160, and 180 deg, respectively. Each case is outlined as follows and is summarized in Table 1 for clarity.

Case No. 1 — Matched-Size Aluminum Welding Wire Dry-Sliding on a Teflon® Wire Liner

An aluminum welding wire was used with a matched size (as recommended by the manufacturer) polymer-based Teflon[2] impregnated wire liner. Experiments were

1. "Cast" refers to the amount of natural curl in the welding wire due to the wrap of the wire onto the spool. "Helix" refers to the amount of natural coil in the welding wire caused by the lateral wrap of the wire from one side of the drum to another.

2. Trade names contained herein are used only to generically identify the material used in this research. Actual welding wire and wire liner compositions are proprietary and hence unknown. Such identification does not constitute recommendation or endorsement of these materials.

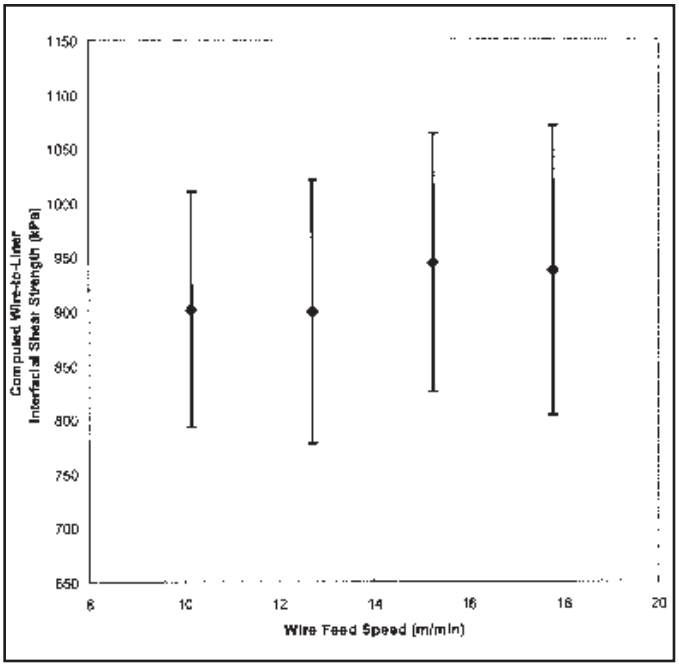

Fig. 9 — Comparison of the interfacial shear strength values as a function of WFS for a 0.8-mm (0.030-in.) ER5356 solid-core aluminum welding wire dry-sliding on a 1.3-mm (0.052-in.) internal diameter Teflon wire liner.

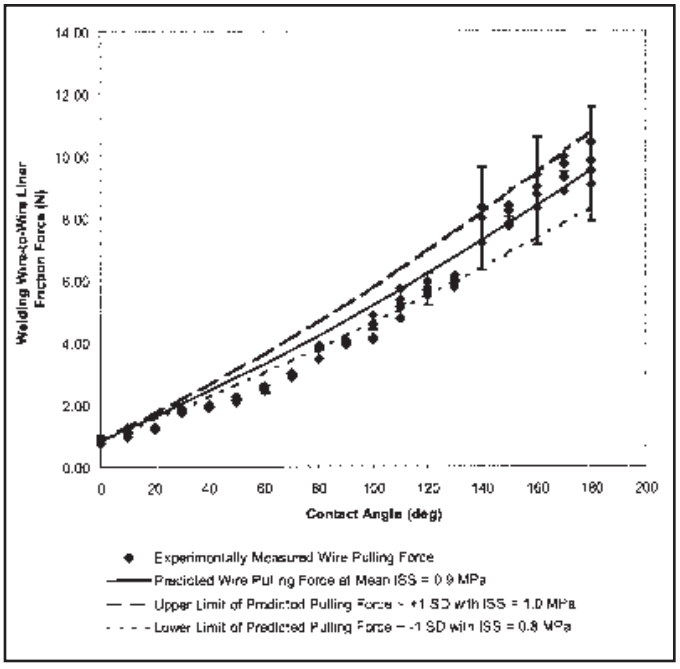

Fig. 10 — Experimental and theoretical comparison using pooled data results for a 0.8-mm (0.030-in.) ER5356 solid-core aluminum welding wire dry-sliding on a 1.3-mm (0.052-in.) internal diameter wire liner. Uncertainty in the model is shown as dashed lines and represents one standard deviation in the estimate of the interfacial shear strength. The data shown have been normalized for a 5-N (1.1-lbf) uniform backtension to show a nonzero force value at zero contact angle representing static friction.

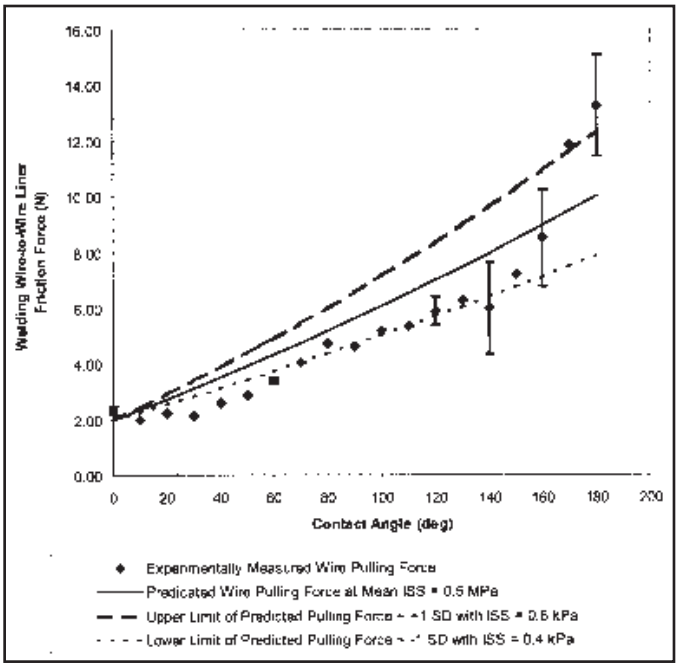

Fig. 11 — Experimental and theoretical comparison using a 1.6-mm (0.0625-in.) ER5356 solid-core aluminum welding wire dry-sliding on a 2.5-mm (0.100-in.) internal diameter Nylon wire liner. Uncertainty in the model is shown as dashed lines and represents one standard deviation in the estimate of the interfacial shear strength. The data shown have been normalized for a 5-N (1.1-lbf) uniform backtension to show a nonzero force value at zero contact angle representing static friction.

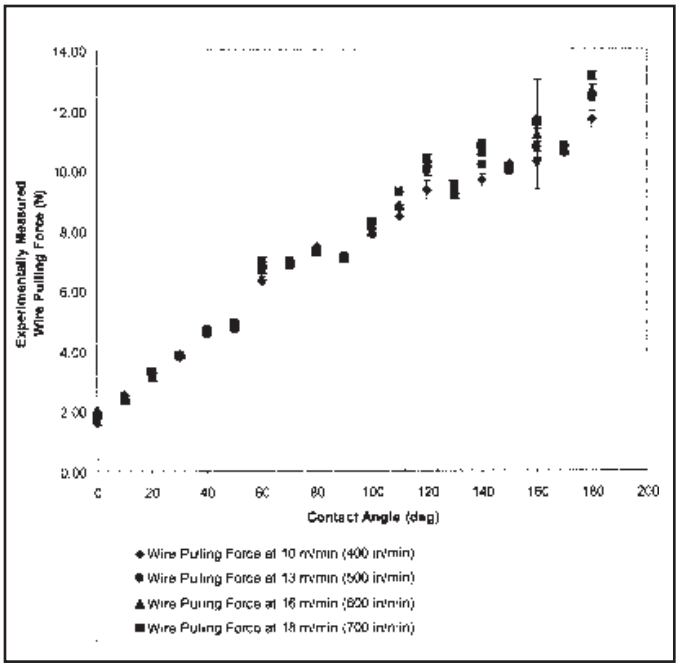

Fig. 12 — Wire pulling force for WFS = 10 to 18 m/min (400 to 700 in./min) with a 1.1-mm (0.045-in.) ES70S6 solid-core copper-clad steel welding wire dry-sliding on a 1.7-mm (0.065-in.) internal diameter spiral wound steel wire liner. The data shown have been normalized for a 10-N (2.2-lbf) uniform backtension to show a non-zero force value at zero contact angle representing static friction.

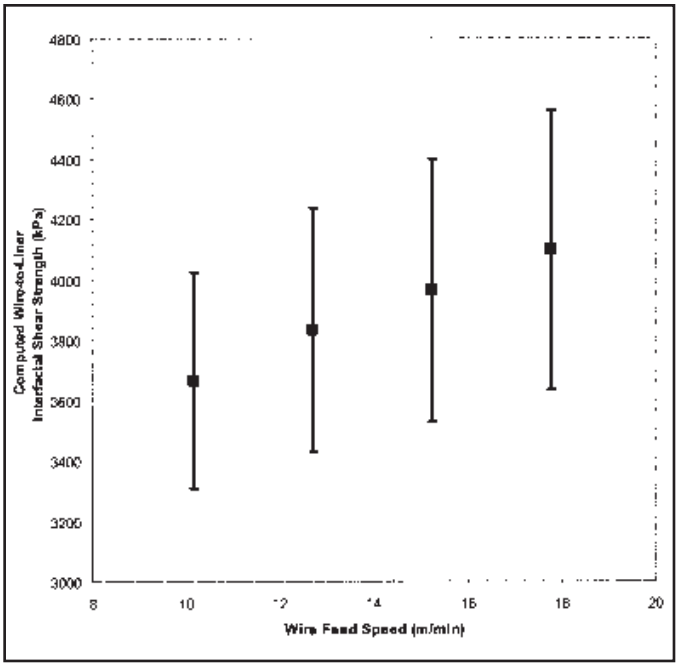

Fig. 13 — Comparison of the interfacial shear strength values as a function of WFS for a 1.1-mm (0.045-in.) ER70S6 solid-core copper-clad steel welding wire dry-sliding on a 1.7-mm (0.065-in.) internal diameter spiral-wound steel wire liner.

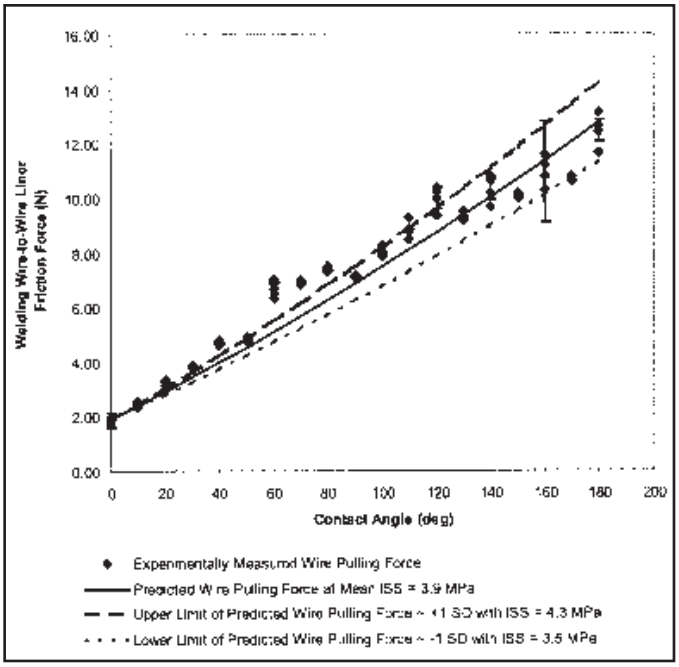

Fig. 14 — Experimental and theoretical comparison using pooled data results for a 1.1-mm (0.045-in.) ER70S6 solid-core copper-clad steel welding wire dry-sliding on a 1.7-mm (0.065-in.) internal diameter spiral-wound steel wire liner. Uncertainty in the model is shown as dashed lines that represent one standard deviation in the estimate of the interfacial shear strength. The data shown have been normalized for a 10-N (2.2-lbf) uniform backtension to show a nonzero force value at zero contact angle representing static friction.

conducted using a 0.8-mm (0.030-in.) ER5356 solid-core aluminum welding wire spooled onto a standard 1-kg (2-lbm) drum. A 2.5 m (8 ft) length of 1.3-mm (0.052-in.) internal diameter "Teflon"[3] wire liner was used and had the manufacturer's rating for use with welding wires ranging from 0.8 to 0.9 mm (0.030 to 0.035 in.) in diameter. This particular combination of welding wire and wire liner provided a diameter ratio of 1.7:1.

Wire feed speeds were varied from 10 to 18 m/min (400 to 700 in./min) in 2.5 m/min (100 in./min) increments to represent the middle range of wire feed rates used during typical aluminum GMAW. Bends in the hose package were simulated by varying the contact angle between the welding wire and the wire liner from 0 to 180 deg in 10-deg increments. A 5-N (1.1-lbf) uniform backtension was applied to the welding wire with the pulley and mass setup to ensure complete contact of the welding wire with the wire liner and to simulate drag normally associated with the wire spool.

3. "Teflon" and "Nylon" have been used as a shorthand notation to refer to the polymer-based, Teflon-impregnated wire liners and the polymer-based, Nylon-impregnated wire liners used in this study.

Case No. 2 — Matched-Size Aluminum Welding Wire Electrode Dry-Sliding on a Nylon Wire Liner

Case No. 2 tested the applicability of the contact model to a larger diameter (≈ 2X larger diameter than that for Case No. 1) aluminum welding wire and polymer-based, Nylon-impregnated wire liner. This study was also conducted to determine whether there was an improvement or degradation in the overall wire feeding performance when using the "Nylon"[3] wire liner.

Experiments were conducted using a 1.6-mm (0.0625-in.) ER5356 solid-core aluminum welding wire spooled onto a standard 1-kg (2-lb) spool. The welding wire was guided through a 2.5 m (8 ft) length of 2.5-mm (0.100-in.) internal diameter Nylon wire liner. This particular size of wire liner was recommended exclusively for use with 1.6-mm-diameter welding wires and provided a diameter ratio of 1.6:1. An intermediate constant-valued WFS of 14 m/min (550 in./min) was selected. This single constant-valued wire feed speed was selected to give a uniform metric of comparison in determining whether there was an increase or decrease in wire pulling force performance when using the Nylon wire liner. The contact angle between the welding wire and the wire liner was similarly varied from 0 to 180 deg in 10-deg increments. A 5-N (1.1-lbf) uniform back-tension was again applied to the welding wire.

Case No. 3 — Matched-Size Copper-Clad Steel Welding Wire Dry-Sliding on a Steel Wire Liner

Case No. 3 was conducted to determine the applicability of the contact model to steel-on-steel GMAW applications when feeding steel welding wires of intermediate diameter through a spiral-wound steel wire liner. Experiments were performed using a 1.1-mm (0.045-in.) ER70S-6 solid-core copper-clad steel welding wire spooled onto a standard 0.5-kg (1-lb) drum. A 2.5 m (8 ft) length of 1.7-mm (0.065-in.) internal diameter spiral-wound steel wire liner was used. This particular liner was recommended for use with welding wires ranging from 0.9 to 1.1 mm (0.035 to 0.045 in.) in diameter and provided a diameter ratio of 1.4:1. Wire feed speeds were similarly varied from 10 to 18 m/min (400 to 700 in./min) in 2.5-m/min (100-in./min) increments, while bends in the hose package were again varied from 0 to 180 deg in 10-deg increments. The uniform backtension on the welding wire was increased to 10 N (2.2 lbf) to compensate for the relatively stiffer steel welding wire.

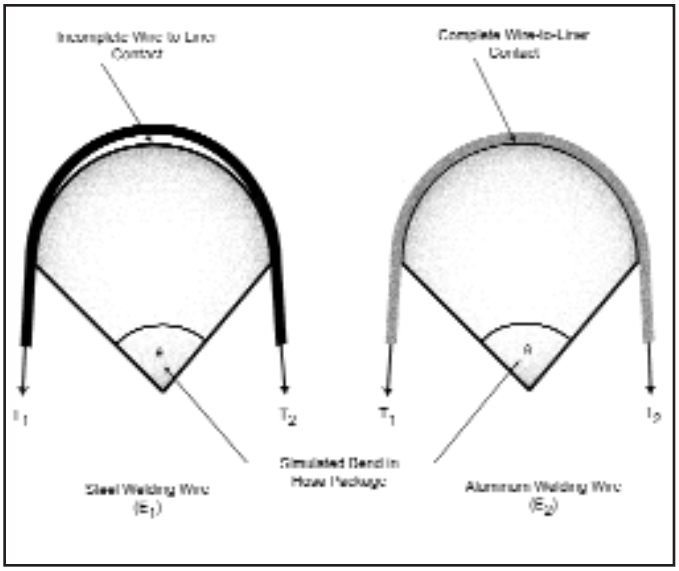

Fig. 15 — Speculated difference in the nature of contact for a steel (stiffer) welding wire vs. an aluminum (more flexible) welding wire.

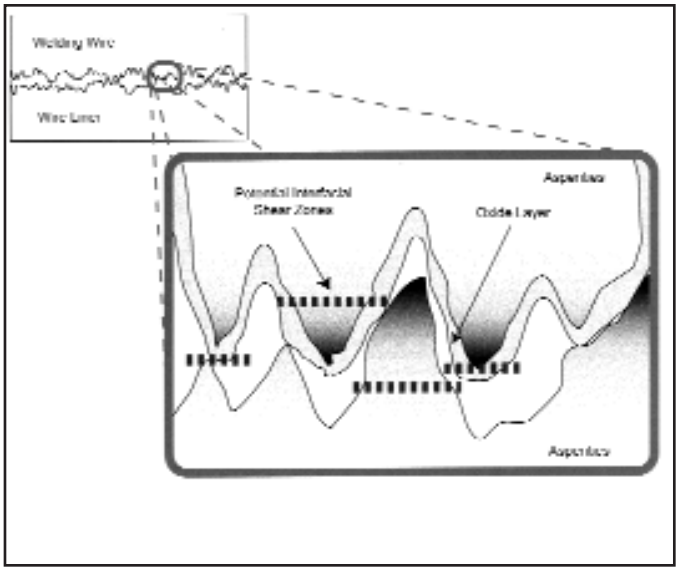

Fig. 16 — Hypothetical mixed asperity-to-asperity contact of the welding wire with the wire liner, showing potential interfacial shear zones.

Results and Discussion

Case Study No. 1 — Matched-Size Aluminum Welding Wire Dry-Sliding on a Teflon Wire Liner

The wire pulling force data (Fig. 5) indicate there is an approximate 2.5:1 exponential increase in wire pulling force as the contact angle between the welding wire and the wire liner is increased from 0 to 180 deg. The severity of the bend in the hose package (i.e., an increase in the angular sum of bend) increases the mean wire pulling force. This corroborates previous research (Ref. 12) that the configuration of the hose package plays a significant role in wire feedability. Normalizing the data set with respect to the applied backtension, the nonzero force value observed at zero contact angle is believed to represent the minimum static friction in the wire-to-liner system. It is believed the static friction component of force is due to self-weight of the welding wire acting against the wire liner and, more predominately, the entry/exit effects of the welding wire passing through the wire liner.

If the data are directly compared against Euler's equation for rope friction (Equation 1) using a representative range of coefficient of friction values ($\mu = 0.2$ to $\mu = 0.4$), the measured wire pulling force can be greatly underestimated or overestimated — Fig. 6.

Here, the representative coefficient of friction values are typical (Refs. 17, 18, 20) and include pairs similar to the tested wire and liner system, such as polymer-on-steel, aluminum-on-Teflon, aluminum-on-Nylon, and Plexiglass-on-steel. A problem with using typical coefficient of friction data is compounded by the wide range of coefficient of friction values that depend on whether the system is lubricated or unlubricated. As a result, it is not clear which coefficient of friction value adequately represents the true welding wire and wire liner system under consideration.

In order to directly compare the experimental results with the contact model, while avoiding the coefficient of friction ambiguity, the "Bootstrap" method (Ref. 21) was used to determine the specific interfacial shear strength (ISS) τ for the tested aluminum-on-Teflon system. In brief, the Bootstrap algorithm is an *n*-iteration method of determining the average value and uncertainty of an unknown model parameter (see flowchart, Fig. 7). The algorithm uses an initial least-squares estimate of the unknown parameter, followed by iteration to generate a secondary guess of the unknown parameter. The secondary guess is based upon a faux data set that has randomly been assigned a residual error computed from the first run. The process is repeated *n* times to give *n* estimates of the unknown parameter, from which a sample average and standard deviation can be computed — Fig. 8. This provides a measurable way of determining the uncertainty in the model. In this case study, 5000 iterations of the Bootstrap algorithm were performed to determine τ and its uncertainty at each of the four wire-feed speeds — Fig. 9.

As indicated in Fig. 9, the value τ is grouped around a central value of 0.9 MPa (130 lb/in.^{2}), prompting a null hypothesis to suggest the interfacial shear strength values (each for a different WFS) originate from the same population, thereby indicating an independence of wire pulling force from wire feed speed. A Chi-Squared goodness-of-fit test was conducted with the interfacial shear strength values using a 95% confidence interval ($\nu = 3$, $\alpha = 0.05$) to yield a computed statistic of 0.262 compared to a critical statistic of 5.991.

Accordingly, the null hypothesis is considered true and indicates the wire pulling force is independent of wire feed speed over the range from 10 to 18 m/min (400 to 700 in./min). As a result, the wire pulling force data of Fig. 5 were pooled as one data set and passed through the Bootstrap algorithm (with $n = 5000$) to generate a new estimate of the interfacial shear strength equal to 0.9 MPa ± 0.1 MPa (130 lb/in.^{2}) for the composite data set.

The interfacial shear strength estimate was subsequently used to compare the pooled data set with the contact model — Fig. 10. Here, the solid line indicates the mean wire pulling force (mean estimate of τ) and the dashed lines indicate the uncertainty in the model based upon the uncertainty in the estimate of the interfacial shear strength. As shown, the contact model is within ± 0.60 N (0.14 lbf) RMS of the measured values and matches the 2.5:1 exponential increase in wire pulling force for all contact angles ranging from 0 to 180 deg.

Case No. 2 — Matched-Size Aluminum Welding Wire Dry-Sliding on a Nylon Wire Liner

Since the results for the aluminum-on-Teflon study indicated the wire pulling

force was independent of wire feed speed, we assumed the same conditions would hold true when testing aluminum-on-Nylon. As a result, a single constant wire feed speed of 14 m/min (550 in./min) was selected for this study to give a uniform metric of comparison of wire pulling force performance when using the Nylon wire liner.

To compare the values of the measured wire pulling force, the aluminum-on-Nylon data were similarly passed through the Bootstrap algorithm to generate a mean interfacial shear strength of 0.5 MPa ± 0.1 MPa (73 lb/in.^{2}±15 lb/in.^{2}). Substituting this computed value of τ into the contact model results in a similar 2.7:1 exponential increase in pulling force when using the 2X larger-diameter welding wire and Nylon wire liner — Fig. 11. The comparison again indicates the severity of the bend (i.e., an increase in the total angular sum of bends) in the hose package plays a significant role toward increasing the overall wire pulling force. In general, the model predicts the wire pulling force to within ± 1.31 N (0.30 lbf) RMS of the measured value. Likewise, the nonzero force component at zero contact angle is again believed to represent the static friction in the wire-to-liner system. In this case, the static friction contribution is twice as large as that of the aluminum-on-Teflon system.

When predicting the wire-to-liner friction, the contact model provides a breadth of distribution that is 50% greater in predicting the wire pulling force when using the welding wire of larger diameter (Fig. 10 vs. Fig. 11). The cause of the larger variation is not known. Despite the increase in uncertainty, the predicted and measured force values for either of the two wire liners (Nylon or Teflon) lie within 20% of each other, with the Nylon wire liner producing the overall larger wire pulling forces for similar contact angles.

Case #3 — Matched-Size Copper-Clad Steel Welding Wire Dry-Sliding on a Steel Wire Liner

Since many of the same aluminum GMAW wire feeding problems are experienced in steel GMAW, Case No. 3 was conducted to assess the contact model in predicting the wire pulling force when using a copper-clad steel welding wire and a spiral-wound steel wire liner. The wire pulling force for a copper-clad steel wire dry-sliding on a steel wire liner is again seen (Fig. 12) to increase as a function of contact angle, but does so nearly linearly ($R^2 = 0.96$) at a rate of 2:1. Again, the data indicate that tighter bends in the hose package increase the wire pulling force.

The Chi-Squared goodness-of-fit test was repeated with the steel-on-steel data sets to again show mathematically (with 95% confidence) that the computed values of interfacial shear strength for each wire feed speed (Fig. 13) originate from the same population as evidenced by a computed Chi-Squared statistic of 3.891 vs. a critical statistic of 5.991. As a result, the wire pulling force for steel-on-steel applications is also shown to be mathematically independent of wire feed speed over the interval of speeds ranging from 10 to 18 m/min (400 to 700 in./min), despite a 10% increase from one wire feed speed to another. Using the pooled data set for steel-on-steel, the mean interfacial shear strength was computed to be 3.9 MPa ± 0.4 MPa (566 lb/in.^{2}±58 lb/in.^{2})

The wire pulling force data were similarly pooled and directly compared with the contact model predictions — Fig. 14. As indicated, the contact model predicts an increase in wire pulling force with increasing contact angle and again suggests that tighter bends in the hose package increase the mean wire pulling force. Likewise, the static friction in the wire and liner system is observed to be similar to that of the aluminum welding wire sliding through the Nylon wire liner.

The increase in wire pulling force in the case of steel-on-steel is observed to increase more linearly than was previously exhibited during the test of aluminum-on-Teflon and aluminum-on-Nylon. Despite this difference, the measured and predicted quantities are within ± 0.80 N (0.18 lbf) RMS of each other. In general, the steel-on-steel results produce mean wire pulling forces that are up to 10% larger than that for either of the two previous aluminum tests.

We speculate that the difference in the observed behavior of the steel and aluminum can be attributed to the nature of the contact between the welding wire and the wire liner. Since Young's modulus of the steel welding wire [$E_{st} \approx$ 200 GPa (30 Mpsi)] is approximately three times that of the aluminum welding wire [$E_{al} \approx$ 73 GPa (10 Mpsi)], under identical applied tensions of T_1 and T_2, welding wires of nominally identical diameter may fail to make complete contact or only make partial contact with the wire liner — Fig. 15. As a result, the loading distribution development (Equation 10) and the resulting governing differential equation (Equation 21) would undoubtedly differ for steel and aluminum conditions, and may account for the observed exponential and linear difference in the data.

We also speculate that the interface between the welding wire and the wire liner plays a significant role in determining the wire pulling force. In all case studies, the computed interfacial shear strength is lower than theoretically expected. Microscopically, the interface between the welding wire and the wire liner can be considered to consist of mixed asperity-to-asperity contacts — Fig. 16. As a result, one of several or a combination of potential shear zones define the true interfacial shear strength.

Although the contact model is developed to account for an "average" interfacial shear strength value over the entire contact region, the theoretical basis of this model only accounts for "bulk" values of the welding wire and the wire liner. Consequently, the contact model does not account for additional intricacies contributed by interactions caused by the oxide layer (if present), lubricant (if present), or any other higher-order factors such as "composite" material values or third-body debris.

Conclusions

1) The welding wire and the wire liner can be modeled as two axially aligned cylinders utilizing aspects of Hertzian contact mechanics and friction theory to compute the interfacial shear strength at the wire/liner interface. The contact model incorporates the bend angle and radius of curvature between the welding wire and the wire liner, as well as nominal diameters and moduli of the welding wire and wire liner.

2) The contact model accurately predicts the wire pulling force for aluminum and steel GMAW applications to within ± 0.60 N (0.14 lbf) RMS and ± 0.80 N (0.18 lbf) RMS, respectively. A statistical analysis has shown with 95% confidence and regardless of liner composition, the wire-pulling force for aluminum-on-Teflon and steel-on-steel GMAW applications is independent of wire feed speed over the interval of speeds ranging from 10 to 18 m/min (400 to 700 in./min).

3) In all tests, the wire-to-liner friction force increases as the severity of the bend in the hose package is increased. This indicates tighter bends in the hose package require larger wire pulling forces to overcome the increased friction. Additionally, the nonzero force component at zero contact angle represents the static friction in the welding wire and wire liner system. When testing aluminum-on-Teflon and aluminum-on-Nylon wire/liner combination, the wire pulling force increased exponentially at a rate of 2.5:1 and 2.7:1, respectively. A 20% larger difference was observed between the mean wire pulling force values when using Nylon-impregnated vs. Teflon-impregnated wire liners. As well, under similar conditions, the wire pulling forces for steel-on-steel wire/liner combination were observed to increase more linearly at a rate of 2:1, and in general were up to 10% larger than either combination of aluminum welding wires.

Acknowledgments

The authors thank the American Welding Society's Graduate Research Fellowship Program and the NIST Professional Research Experience Program (PREP) for project funding. The authors also extend their most sincere thanks to Dr. Tom Siewert of NIST and to Mr. John Hinrichs of Friction Stir Link, Inc., for their practical insight and advice into this research.

References

1. Quinn, T. P. 2002. Process sensitivity of GMAW: aluminum versus steel. *Welding Journal* 81(4): 55-s to 64-s.

2. Rudy, J. F., Brown, D. C., and Groth, W. G. 1966. Study of current contact tubes for gas metal arc welding. *Welding Journal* 45(8): 374-s to 378-s.

3. Yamada, T., and Tanaka, O. 1987. Fluctuation of the wire feed rate in gas metal arc welding. *Welding Journal* 66(9): 35–42.

4. Quinn, T. P., Madigan, R. B., Mornis, M. A., and Siewert, T. A. 1995. Contact tube wear detection in gas metal arc welding. *Welding Journal* 74(4): 115-s to 121-s.

5. Samokovliisky, D. A. 1986. Wire feed systems for robotic MIG welding. *Metal Construction* 18(5): 293–296.

6. Nichols Research Corp (NRC). 1992. Development of an automated wire delivery system for robotic welding applications. NASA-CR-194216: 37p.

7. Kuvin, B. F. 1998. New wire feeders deliver the goods. *Welding Design and Fabrication* 71(2): 29–32.

8. Villafuerte, J. 1999. Understanding contact tip longevity for gas metal arc welding. *Welding Journal* 78(12): 29–35.

9. Almy, D. 2000. Wire-feed upgrade drives aluminum-welding productivity. *Metal Forming* 34 (4): 28–32.

10. Hinrichs, J. F. 1998. What's wrong with gas metal arc welding (GMAW)? Draft Revision 4: The Welding Link.

11. Hinrichs, J. F., Noruk, J. S., McDonald, W. M., and Heideman, R. J. 1995. Challenges of welding aluminum alloys for automotive structures. *Svetsaren* 50(3): 7–9.

12. Dilthey, U., and Reisgen, U. 1995. Tests on wire feed systems for gas metal-arc welding. *Welding and Cutting* 47(1): E12–E14.

13. Euler, L. 1762. Remarques sur l'effet du frottement dans l'equilibre. *Memoires de l'Academie des Sciences de Berlin*. pp. 265–278.

14. Padilla, T. M. 2001. A mathematical model of wire feeding mechanisms in gas metal arc welding. M.S. Thesis. Colorado School of Mines, Golden, Colo.

15. Greenwood, J. A., and Williamson, J. B. P. 1996. The contact of nominally flat surfaces. *Proceedings of the Royal Society: London*, Vol. 295, Series A: 300–319.

16. Edwards, C. H., and Penney, D. E. 1990. *Calculus and Analytical Geometry,* 3rd ed. New Jersey: Prentice Hall, Inc.

17. Williams, J. A. 1996. *Engineering Tribology*. New York: Oxford University Press Inc.

18. Bowden, F. P., and Tabor, D. 1950. *The Friction and Lubrication of Solids*, Vol. 1. Oxford Press.

19. Childs, T. H. C. 1980. The contact and friction between flat belts and pulleys. *International Journal of Mechanical Science* 22: 117–126.

20. Marks, L. S. 1916. *Standard Handbook for Mechanical Engineers*. New York, N.Y.: McGraw-Hill.

21. Bradley, E. 1982. The Jack Knife, the Bootstrap and other resampling plans. Society for Industrial and Applied Mathematics, *CBMS-NSF Regional Conference Series in Applied Mathematics.* Philadelphia, Pa., 38 p.